DNS, LES, and wall-modeled LES of separating flow over periodic hills

By P. Balakumar†, G. I. Park AND B. Pierce

Separating flow in a channel with streamwise periodic constrictions is investigated using direct numerical simulation (DNS), large eddy simulation (LES), and wall-modeled LES (WMLES). The Reynolds number based on the hill height and the bulk velocity above the hill crest is 10,595. The results presented include mean velocities, Reynolds stresses, and separation/reattachment points. High-resolution DNS shows very good agreement with the reference experiment. Despite the very coarse resolution, the results from WM-LES with three different wall models are comparable to those from the DNS and the experiment.

1. Introduction

Turbulent flow is characterized by the existence of a vast range of length and time scales ranging from the smallest, the Kolmogorov scale, to the largest, determined by the geometry. The computer resources and time constraints required to obtain numerical solution of the Navier-Stokes equations for high Reynolds number turbulent flows are still prohibitive. Hence, the current state of the art is to solve some approximate versions of the Navier-Stokes equations with turbulence modeling. The simplest and the most popular approximate method is the set of Reynolds-Averaged Navier-Stokes (RANS) equations, where the equations are derived for time- or ensemble-averaged quantities. However, prediction of separated flows with existing RANS turbulence models is still unsatisfactory. Often, incipient separations are suppressed severely, and RANS tends to overpredict the size of the separation bubble when the flow separates massively and then reattaches by the change of geometries. Examples include various RANS model validation cases investigated at NASA Langley, such as a two-dimensional hump, the 2-D periodic hill, and the 3-D Ahmed body. The second approximate method uses the large eddy simulation (LES) equations, which are solved for the large-scale motions resolved by the underlying grid. The unknown stresses associated with the subgrid-scale (SGS) motions are modeled to close the equations. In order for LES to be accurate, the dynamically important motions in the flow have to be sufficiently resolved. This requirement is hard to meet in high Reynolds number wall-bounded flows, and application of LES at realistic Reynolds numbers often requires wall-modeling, a less costly approach to model the effect of wall-layer dynamics on the outer-layer flow. Although wall-resolved LES has proven its predictive capability in a number of separating flows, it is not clear to what degree under-resolved LES or wall-modeled LES can predict separated flows with reasonable accuracy.

The objective of the present work is to perform wall-resolved and wall-modeled LES simulations of flow through a periodic channel with constrictions (separated flow over a 2-D hill) and to compare them to DNS and experimental results. Despite the simple

† NASA Langley Research Center

geometry, the case chosen possesses flow phenomena critical in assessing the predictive capability of (WM)LES, such as turbulent separation and reattachment. The fact that detailed documentation of experiments is available (from low to high Reynolds numbers) is also a merit.

2. Flow configuration

The size of the computational domain is $L_x = 9h$, $L_y = 3.035h$, and $L_z = 4.5h$ in the streamwise (x), wall-normal (y), and spanwise (z) directions, respectively, where h is the height of the hill. The hill crest is located at $(x/h, y/h) = (0, 1)$. Stationary solid walls are located at the bottom and top of the domain (see Figure 1). Periodic boundary conditions are applied in the streamwise and spanwise directions. The Reynolds numbers based on the hill height (h), the kinematic viscosity (ν), and the average velocity above the hill crest ($U_{\mathcal{S}}$) is $\mathrm{Re}_{\mathcal{S}} = U_{\mathcal{S}}h/\nu = 10{,}595$. The Reynolds number at the hill crest ($\mathrm{Re}_{\mathcal{S}}$) is related to the bulk Reynolds number $\mathrm{Re}_{\mathcal{B}}$ ($= U_{\mathcal{B}}h/\nu$) by

$$\mathrm{Re}_{\mathcal{B}} = \Gamma \mathrm{Re}_{\mathcal{S}}, \tag{2.1}$$

where $U_{\mathcal{B}}$ is the domain-averaged bulk velocity and Γ is a geometric factor given by

$$\Gamma = \frac{L_y(x=0)}{\frac{1}{L_x}\int_0^{L_x} L_y(x)dx} = 0.72. \tag{2.2}$$

In order to drive the flow in a periodic channel at a fixed $Re_{\mathcal{S}}$ (i.e., constant mass flow rate), a spatially uniform but time-varying body force term $f_{\rho u}$ is added to the right-hand side (RHS) of the streamwise momentum equation

$$f_{\rho u}(t) = \frac{1}{\mathcal{V}}\int_{walls}(pn_1 - \sigma_{1j}n_j)dA, \tag{2.3}$$

where $\mathcal{V}$ is the volume of the computational domain, p is the pressure, σ_{ij} is the viscous stress tensor, and n_j is the j^{th} component of the outward normal vector. This term balances the boundary force exactly, and keeps $U_{\mathcal{B}}$ constant in time. Time-variation of $U_{\mathcal{S}}$ was less than 1%, and therefore the simulations are run at almost constant $\mathrm{Re}_{\mathcal{S}}$ by fixing $\mathrm{Re}_{\mathcal{B}}$. In compressible calculations, the bulk Mach number is set to 0.2 to allow comparison to incompressible calculations and the experiment. The work done by the body force on the fluid is accounted for by adding a consistent source term $f_{\rho E} = uf_{\rho u}$ to the RHS of the total energy equation. Simulation results are compared to the water channel experiment of Breuer *et al.* (2009) available as a ERCOFTAC database at http://qnet-ercoftac.cfms.org.uk/w/index.php/UFR_3-30_Test_Case.

3. Description of mesh parameters, solvers, and models

Table 1 summarizes the information of the present periodic hill simulations using different flow solvers and wall treatments. In the DNS, the maximum grid spacings in the x- and z-directions are $\Delta x^+ = 4$ and $\Delta z^+ = 3$, respectively. The minimum wall-normal grid spacing at the wall varies between $\Delta y^+ = 0.1$ to 0.3, and the maximum wall-normal spacing in the middle of the channel is $\Delta y^+ = 4$. The WMLES mesh is designed to resolve only the large-scale eddies in the outer layer, and the grid spacings scale not with the viscous wall unit, but with the boundary layer thickness. Consequently, the number of cells in the WMLES is significantly less than that in the DNS. It should

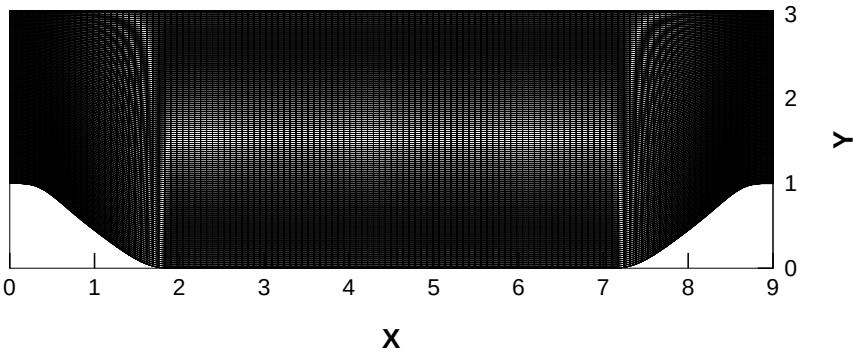

FIGURE 1. Side view of the mesh used for LES and WMLES calculations.

Case	Simulation	(N_x, N_y, N_z)	N_{cells}	Solver	Wall model
1	DNS	$(800, 500, 500)$	200M	structured (7^{th}-order WENO)	N/A
2	LES	$(197, 197, 144)$	5.58M	structured (6^{th}-order compact)	N/A
3	ILES	$(197, 197, 144)$	5.58M	structured (6^{th}-order compact)	N/A
4	WMLES	$(128, 128, 72)$	1.18M	Vida (2^{nd}-order central)	Slip WM
5	WMLES	$(128, 128, 72)$	1.18M	CharLES (2^{nd}-order central)	Non-equil. WM
6	WMLES	$(128, 128, 72)$	1.18M	CharLES (2^{nd}-order central)	Equil. WM

TABLE 1. Information of periodic hill simulations. All cases except for case 4 are compressible flow simulations. CharLES and Vida solvers are provided by Cascade Technologies, Inc.

also be noted that the grid points in the DNS are clustered near the walls to resolve the sharp velocity gradient in the wall-normal direction, whereas the WMLES mesh has uniform grid spacing in the wall-normal direction (on the hill crest, $\Delta y/h = 4 \times 10^{-4}$ in the DNS, and $\Delta y/h = 2 \times 10^{-2}$ in the WMLES).

3.1. *Solver information*

The structured solver used for cases 1, 2, and 3 employs the high-order compact schemes of Lele (1992) and WENO. The DNS is calculated exclusively with a 7th-order WENO scheme. For the (I)LES calculations, an 8th-order spatial discretization is used in the periodic directions, and a 6th-order scheme is used in the wall-normal directions. Additionally, an implicit compact 8th-order filtering is used to remove the high-frequency oscillations. The filter was applied every 10 time-steps. The solution method implemented is described in Balakumar (2009). The dynamic Smagorinsky model with a least-squares procedure for computation of model coefficients is used for the LES subgrid-scale (SGS) closure (Germano *et al.* 1991; Lilly 1992). ILES is run with no SGS model.

CharLES, a cell-centered unstructured finite volume compressible LES solver, is used for cases 5 and 6. The spatial discretization on a regular grid is central and formally 4th-order accurate on a Cartesian equidistant grid, but it reduces to 2nd-order accurate on arbitrary unstructured meshes. In regions with poor grid quality, the central flux is

blended with the HLLC Riemann flux in a minimally dissipative manner for numerical stability (see Khalighi *et al.* 2011 and Park 2014 for the details). A compressible dynamic Smagorinsky model of Moin *et al.* (1991) with the modification of Lilly (1992) is used for the SGS closure. The incompressible calculation (case 4) is performed with Vida, an edge-based unstructured finite volume incompressible LES solver. The dynamic Smagorinsky model with a least-squares procedure for computation of model coefficients is used for the LES SGS closure (Germano *et al.* 1991; Lilly 1992).

3.2. *Wall models*

Three wall models developed in CTR are employed in coarse wall-modeled LES calculations. These models are the non-equilibrium wall model of Park & Moin (2014), the equilibrium wall model of Bodart & Larsson (2011), and the dynamic slip-velocity model of Bose & Moin (2014).

In the non-equilibrium wall model, unsteady 3-D RANS equations are solved on an embedded, thin mesh that covers the inner layer to provide wall stress (τ_w) and heat flux (q_w) to the LES. The non-equilibrium wall model has its own computational domain in the near-wall region on which three-dimensional, time-dependent flow equations are solved. Top boundary conditions in the wall model are imposed by instantaneous LES state variables. The primal LES solver and the wall model therefore have the same degree of complexity, and they have to be integrated in time synchronously while exchanging the boundary conditions. The equilibrium wall model is derived from the non-equilibrium wall model by neglecting all terms except for those pertaining to the wall-normal diffusion. The equilibrium wall model reduces to a system of uncoupled ordinary differential equations (ODE) and is therefore computationally very efficient. However, it may have limitations in non-equilibrium flows since unsteady advection and pressure gradient terms are all neglected. Note that in both approaches the near-wall turbulence in the primal LES grid (albeit underresolved) is still largely dictated by the LES, since the modeled fluxes enter the LES domain as approximate boundary conditions only. This is in contrast to detached eddy simulation and hybrid LES/RANS in which the outer LES solution is explicitly linked to the low-fidelity near-wall RANS solution at the governing equation level.

In the dynamic slip-velocity wall model, a Robin-type slip-wall boundary condition for WMLES is obtained directly from the derivation of the LES equations using a differential filter

$$\overline{u}_i - (C\bar{\Delta}_w)\frac{\partial \overline{u}_i}{\partial n} = 0, \qquad i = 1, 2, 3, \tag{3.1}$$

where $\overline{u}_i$ is the filtered velocity, n is the wall-normal direction, and $C\bar{\Delta}_w$ is the model coefficient determined by a dynamic procedure. Equation (3.1) was derived by requiring the filtered velocity field to obey the exact definition of the differential filter at the wall. This type of wall model is potentially very attractive, since the additional cost of wall-modeling is negligible compared to traditional wall models, and since the model is free of any *a priori* specified coefficients. As the model is derived from purely mathematical considerations, its performance is being further investigated at CTR for both canonical and complex wall-bounded flows.

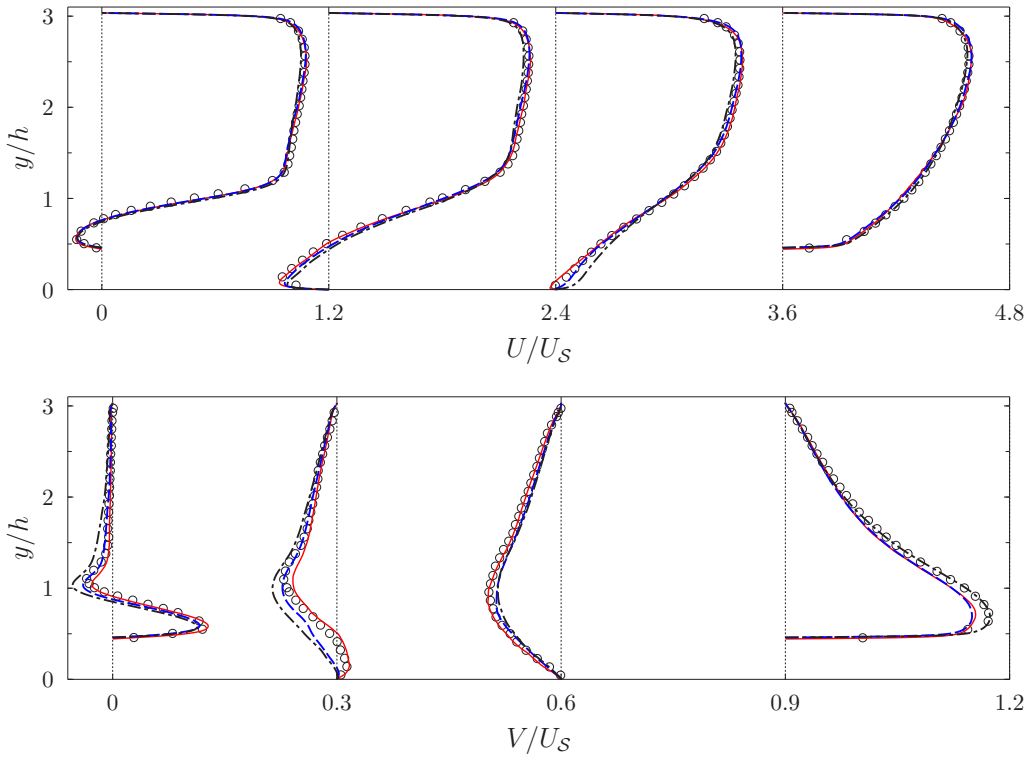

FIGURE 2. Mean velocity profiles in the streamwise (U) and vertical (V) directions (color online). From left to right, velocity profiles at $x/h = 1, 2, 4$, and 8. Red solid lines, DNS (case 1); blue dashed lines, LES (case 2); black dash-dotted lines, ILES (case 3); circles, experiment (Breuer *et al.* 2009).

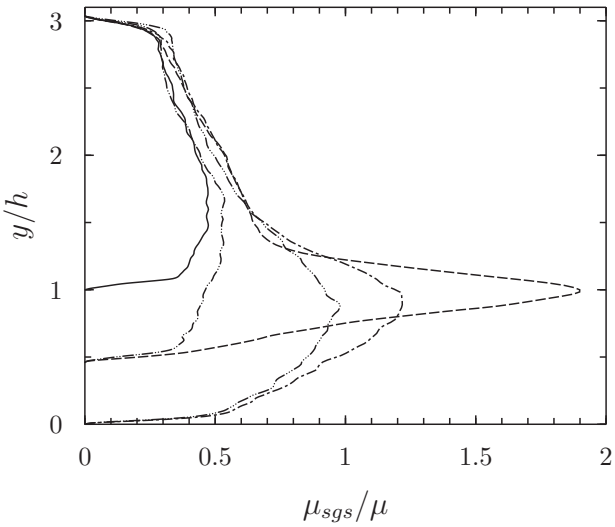

FIGURE 3. Variation of the SGS eddy viscosity at different stations (case 2). Solid line, $x/h = 0$; dashed line, $x/h = 1$; dash-dotted line, $x/h = 2$; dash-dot-dot-dotted line, $x/h = 4$; dash-dot dotted line, $x/h = 8$.

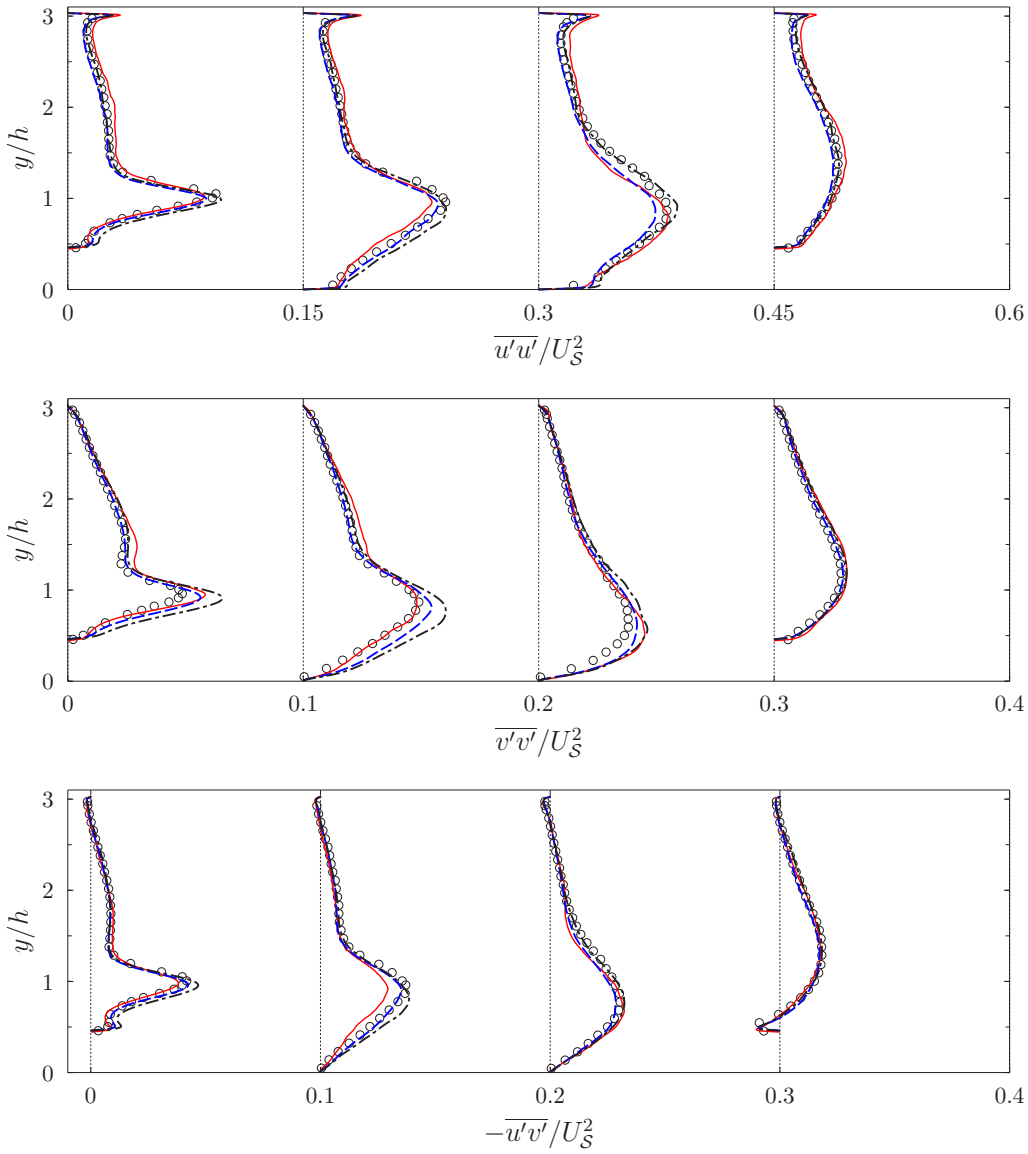

FIGURE 4. Profiles of Reynolds stresses at $x/h = 1, 2, 4$, and 8 (from left to right, color online). Red solid lines, DNS (case 1); blue dashed lines, LES (case 2); black dash-dotted lines, ILES (case 3); circles, experiment (Breuer *et al.* 2009).

4. Results

4.1. *DNS, LES, and ILES results (high-order structured solvers)*

Figures 2-4 show the mean velocity profiles and the turbulent statistics obtained from DNS (case 1), LES with the dynamic Smagorinsky model (case 2), and ILES without the SGS model (case 3). The reattachment point is located at $x_{reatt} = 4.5$, 4.1, and 3.7 from the DNS, LES, and ILES, respectively. Figure 2 depicts the comparison of the mean velocity profiles obtained from the three simulations at different streamwise locations x= 1, 2, 4, and 8. We also included the experimental results of Breuer *et al.* (2009).

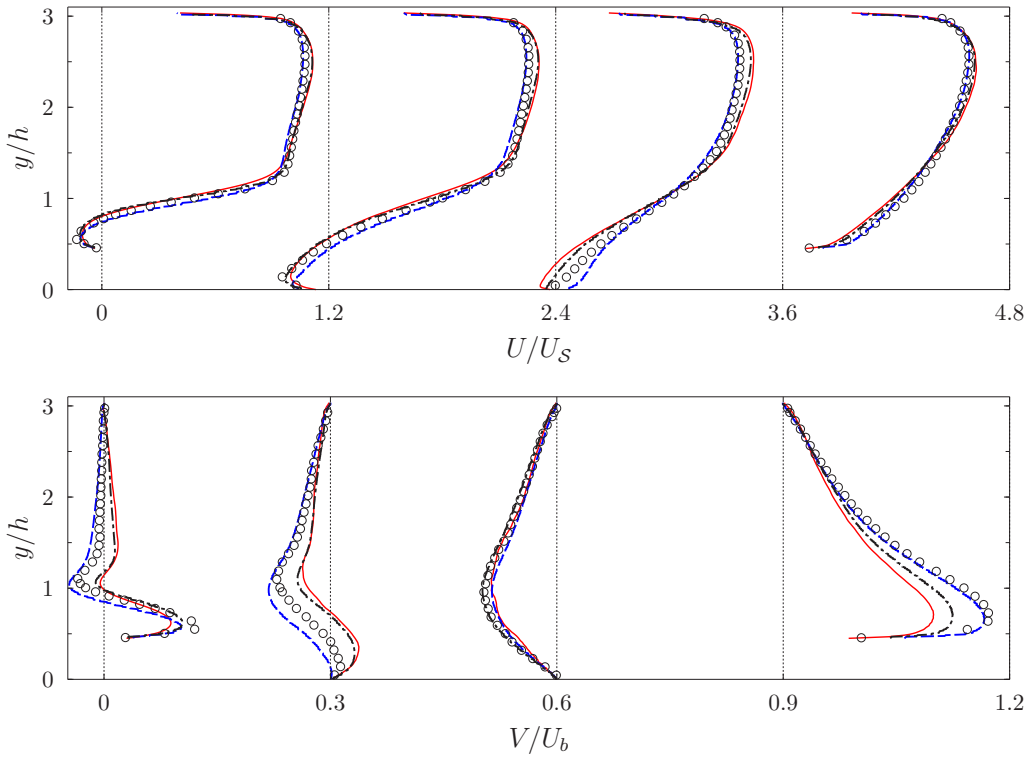

FIGURE 5. Mean velocity profiles in the streamwise (U) and vertical (V) directions (color online). From left to right, velocity profiles at $x/h = 1, 2, 4$, and 8. Red solid lines, slip WM (case 4); blue dashed lines, non-equilibrium WM (case 5); black dash-dotted lines, equilibrium WM (case 6); circles, experiment (Breuer *et al.* 2009).

The agreement among the profiles obtained from the DNS, ILES, LES simulations and the experiment are quite good. Figure 3 shows the variation of the ratio of the subgrid eddy viscosity to the molecular viscosity at the same probe stations. As expected, the eddy viscosity is large in the separated shear layer region. The ratio is about μ_{sgs}/μ = 0.50 near the separation point $x \approx 0$, peaks to a value of about μ_{sgs}/μ =1.9 near $x \approx 1$, and decreases to about μ_{sgs}/μ =1.0 near the attachment point $x \approx 4$. Hence the maximum SGS contribution is about twice the laminar viscosity, and this occurs immediately downstream of the separation point. Figure 4 depicts the comparison of Reynolds stresses ($\overline{u'u'}$, $\overline{v'v'}$, and $\overline{u'v'}$) obtained from the three simulations.

4.2. *WMLES results (2nd-order unstructured solvers)*

Mean velocities and Reynolds stresses from the WMLES calculations are compared to the experiment in Figures 5 and 6, respectively. Despite the very coarse grid resolution and low-order spatial discretization, the agreement between the wall-model predictions and the measurement is reasonably good. The slip wall model (case 4) and the equilibrium wall model (case 6) give almost identical results, and overpredict the size of the separation bubble (stronger separation). On the contrary, the bubble size is underpredicted (faster recovery) with the non-equilibrium wall model (case 5). In general, the velocity profiles from the non-equilibrium wall model show better agreement with the experiment than

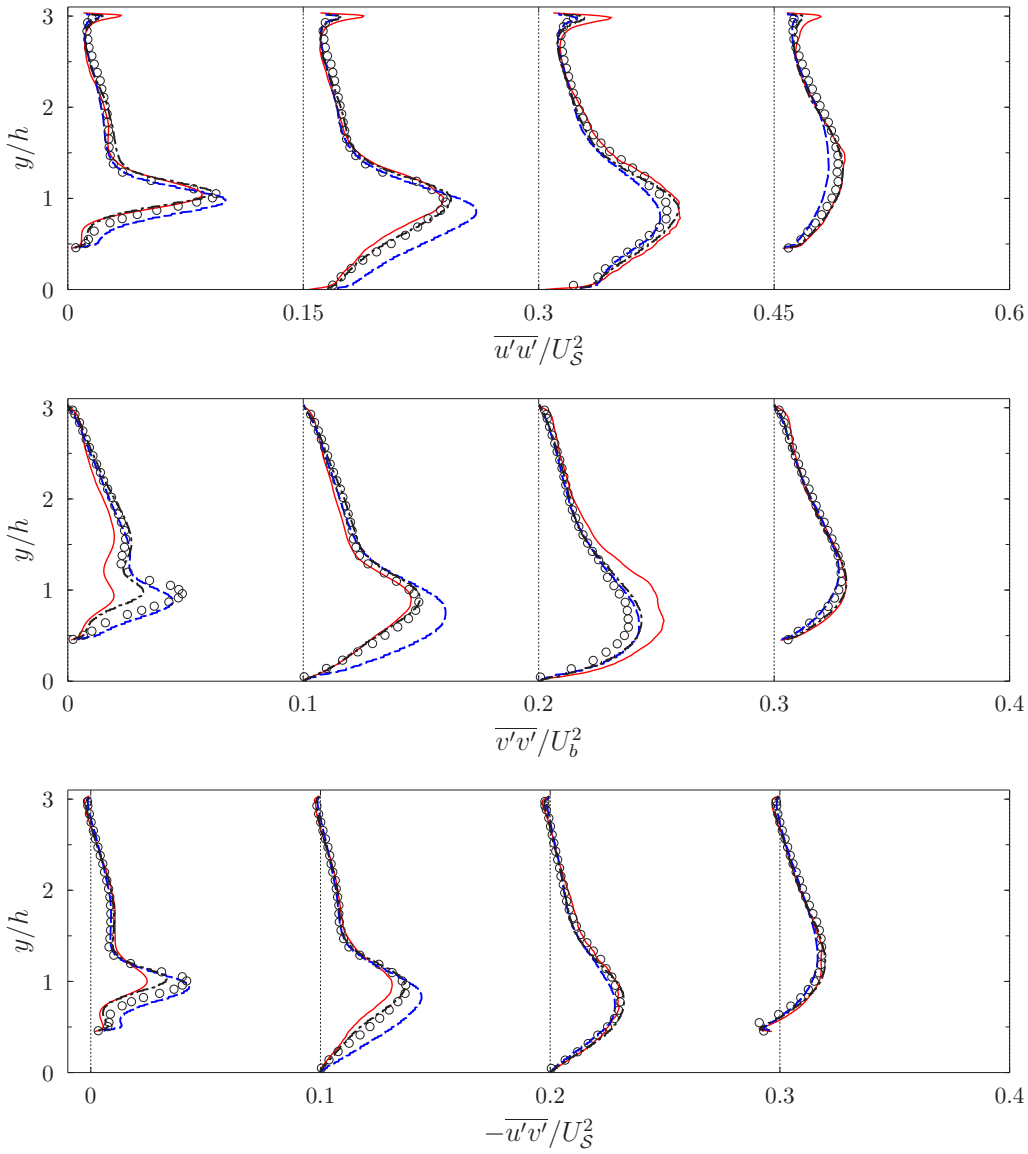

FIGURE 6. Profiles of Reynolds stresses at $x/h = 1, 2, 4$, and 8 (from left to right, color online). Red solid lines, slip WM (case 4); blue dashed lines, non-equilibrium WM (case 5); black dash-dotted lines, equilibrium WM (case 6); circles, experiment (Breuer *et al.* 2009).

the profiles from the other two models, but the difference is not pronounced enough to state which wall model outperforms the others.

5. Conclusions

DNS, LES, and wall-modeled LES are carried out for a flow through a channel with streamwise-periodic constrictions at $\mathrm{Re}_S = 10{,}595$. The DNS and the resolved LES are performed with a high-order structured code, and the wall-modeled calculations are run

with second-order unstructured finite volume codes. The mean flow and the turbulent quantities from the DNS and the resolved LES agree well with the experiment. The computed eddy viscosity in the resolved LES shows that the effect of the SGS model is marginally significant for the grids and the algorithm used in the simulations. Despite being significantly under-resolved, WMLESs with three different wall models (non-equilibrium, equilibrium, and slip WMs) predict the mean flow field with reasonable accuracy. Simulations at a higher Reynolds number, $\mathrm{Re}_{\mathcal{S}} = 37{,}000$, are planned in follow-up studies.

Acknowledgments

We gratefully acknowledge the generous support of Center for Turbulence Research during the Summer Program. Additionally, George Park was supported by NASA under the Subsonic Fixed-Wing Program (Grant No. NNX11AI60A), and Brian Pierce was supported by Stanford Graduate Fellowship. All wall-modeled LES calculations were carried out on the US Department of Energy's advanced computational facilities (Pinto and Moonlight clusters) at Los Alamos National Laboratory.

REFERENCES

Balakumar, P. 2009 Receptivity of a supersonic boundary layer to acoustic disturbances. *AIAA J.* **47**, 1034–1041.

Bodart, J. & Larsson, J. 2011 Wall-modeled large eddy simulation in complex geometries with application to high-lift devices. *Annual Research Briefs*, Center for Turbulence Research, NASA Ames/Stanford University pp. 37–48.

Bose, S. T. & Moin, P. 2014 A dynamic slip boundary condition for wall-modeled large-eddy simulation. *Phys. Fluids* **26**, 015104.

Breuer, M., Peller, N., Rapp, C. & Manhart, M. 2009 Flow over periodic hills – numerical and experimental study in a wide range of Reynolds numbers. *Comput. Fluids* **38**, 433–457.

Germano, M., Piomelli, U., Moin, P. & Cabot, W. 1991 A dynamic subgrid-scale eddy viscosity model. *Phys. Fluids A* **3**, 1760–1765.

Khalighi, Y., Nichols, J. W., Ham, F., Lele, S. K. & Moin, P. 2011 Unstructured large eddy simulation for prediction of noise issued from turbulent jets in various configurations. *AIAA Paper No. 2011-2886*.

Lele, S. K. 1992 Compact finite difference schemes with spectral-like resolution. *J. Comput. Phys.* **103**, 16–42.

Lilly, D. K. 1992 A proposed modification of the Germano subgrid-scale closure method. *Phys. Fluids* **4**, 633–635.

Moin, P., Squires, K., Cabot, W. & Lee, S. 1991 A dynamic subgrid-scale model for compressible turbulence and scalar transport. *Phys. Fluids* **3**, 2746–2757.

Park, G. I. 2014 *Wall-modeled large eddy simulation in an unstructured mesh environment.* Ph.D. Thesis, Stanford University.

Park, G. I. & Moin, P. 2014 An improved dynamic non-equilibrium wall-model for large eddy simulation. *Phys. Fluids* **26**, 015108.